GT2010-23(&)

FULL SCALE WIND TURBINE FLOWFIELD MEASUREMENTS USING A 7-SENSOR FAST RESPONSE PROBE

M. Mansour, G. Kocer, C. Lenherr, N. Chokani, R.S. Abhari
Laboratory for Energy Conversion
Department of Mechanical and Process Engineering
ETH Zürich, Switzerland

ABSTRACT

The unsteady wind profile in the atmospheric boundary layer upstream of a modern wind turbine is measured. The measurements are accomplished using a novel measurement approach that is developed and demonstrated for wind energy applications. The measurements of the unsteady 3D velocity field have to be resolved in a low dynamic head environment and over large flow angles around a modern wind turbine (rotor diameter 80-120m and tower height 60-100m). The novel measurement approach is comprised of an autonomous Uninhabited Aerial Vehicle (UAV) that is equipped with a seven-sensor fast-response aerodynamic probe (F7S-UAV). The autonomous UAV enables high spatial resolution (~9% of rotor diameter) measurements, which hitherto have not been accomplished around full-scale wind turbines. The 7-sensor fast-response aerodynamic probe developed at ETH Zurich is the key-enabling technology for the measurements. This measurement system is realized as a light, compact measurement chain that conforms to the limited payload area and weight restrictions of the UAV. The time-averaged wind profile from the F7S-UAV probe is found to be in very good agreement to an independently measured profile using the UAV. This time-averaged profile, which is measured at a wind turbine that is located in moderately complex terrain, differs by as much as 30% from the wind profile that is extrapolated from a logarithmic height formula; therefore the limited utility of extrapolated profiles, which are commonly used in site assessments, is made evident. The time-varying wind profiles show that, at a given height, the velocity fluctuations can be as much as 44% of the time-averaged velocity, therefore indicating that the wind turbine and its components, notably the gearbox, will experience substantial loads that may impact the fatigue life of the components. Furthermore, the shear in the velocity profile also subjects the fixed pitch blade to varying incidences and loading. Analysis of the associated velocity triangles indicates that the sectional lift coefficient at mid-span of this modern turbine would vary by 12% in the measured time-averaged wind profile. These variations must be accounted in the structural design of the blades. Thus the measurements of the unsteady wind profile accomplished with this novel measurement system, demonstrate that it is a cost effective complement to the suite of available site assessment measurement tools.

NOMENCLATURE

h	hour
min	minute
p	pressure
r	radial potion
t	time
v	absolute velocity
z_o	roughness factor
H	height
K	polynomial coefficient
R	turbine blade radius
U	voltage
T	temperature

Greek:

α	incidence angle
θ	pitch angle
ψ	yaw angle
ω	angular velocity

Superscripts:

$\overline{}$	average

INTRODUCTION

Over the last decade, the global wind industry has experienced exponential growth; the annual increase in installed capacity averages 24%. In 2008, the new installed wind capacity led all new electric generating capacity (even ahead of new natural gas) in both EU and U.S., accounting for 38% and 42% of all new electric generating capacity, respectively in the world's leading regional and national markets for wind power. The growth of wind generated electricity is driven by its many benefits including no CO_2 emissions, no water consumption for electricity generation, security of energy supply through increasingly diversified electrical energy mix, and major economic impact (in 2008, €36billion new power generation equipment and more than 400'000 jobs in the global wind industry). The continued rapid development of wind energy projects requires improved approaches to site assessment, such that the acquisition time of the wind resource is reduced for wind farm developers and the placement of wind turbines is optimized for wind farm operators.

Until now site assessment is most commonly performed using a mast-mounted cup anemometer, which offers a robust and simple solution[1]. Due to the rapid increase in turbine size over the past years, with typical hub heights often exceeding 90m, the mast mounted-cup anemometers have shown their limits. The erection of higher mast-anemometer leads to onerous installation and maintenance costs for the developer of a wind energy project. Moreover this technique offers only a few discrete points of measurements, which is insufficient to assess accurately the wind profile, and thus the expected annual energy yield for wind turbines that are located in moderately and highly complex terrains. A further

limitation is that the current understanding of flows around full-scale wind turbines is largely derived from point measurements obtained from a few widely scattered masts. These point measurements are insufficient to improve the understanding and comprehension of interaction between a large modern wind turbine (rotor diameter 80-120m) and turbulent atmospheric boundary flow (thickness 200-1500m). A more detailed understanding of the turbulent flows upstream, as well as downstream, of the wind turbines is required. Recently, substantial efforts have focused on the use of light detection and ranging (LIDAR) measurement systems in wind energy applications [2-4], whereas previous applications of LIDAR have been in aerospace applications [5, 6]. However short range LIDAR profilers are limited to observations up to 200m along a single line, and are therefore not cost effective solutions to detail the 3D flowfield around wind turbines. To overcome this limitation 3-D "windscanners" have been developed either by having a system that scans the transmitted beam over 360° in azimuth [7] and for various heights or by having a set of three steerable Doppler LIDARs [8]. Their drawback is the prohibitive system cost and limited flexibility in transportation and set-up.

The objective of this paper is to assess the use of an instrumented UAV to provide wind measurements in wind energy projects. This assessment is part of recently developed multi-faceted wind energy program at ETH Zurich. The components of this program include econometric modeling, computational fluid dynamic modeling, sub-scale wind turbine experiments, and full-scale experiments on wind turbines. The purpose of the sub-scale and full-scale experiments is to provide detailed flowfield data that can used to enhance and validate the computational models. Therefore the specific goal of the current project is to develop a light, mobile, cost effective measurement system that can be used either to provide time-resolved wind measurements around full-scale wind turbine or complementary wind profile measurements for site assessment. UAVs fulfill the requirement of being lightweight, mobile, and cost effective and have proven their reliability in several meteorological measurement campaigns [9, 10]. In order to provide wind measurements on such a platform, the key enabler is the fast-response aerodynamic probe technology that has been developed at ETH Zurich for turbomachinery applications. The adaptation, development, integration and demonstration of this technology for use on a UAV to provide time-resolved wind profile measurements in full-scale wind turbine applications is the subject of this paper. In the subsequent sections, the design and calibration of the seven-sensor fast-response aerodynamic probe as well as its integration in the UAV are presented in detail. Then wind profile measurements results performed upstream of a wind turbine are presented and discussed.

7S-FRAP TECHNIQUE

The principal component for time-resolved wind measurements is the 7-sensor fast-response aerodynamic probe (7S-FRAP). The probe is based on previous turbomachinery applications in the Laboratory for Energy Conversion at the Swiss Federal Institute of Technology Zürich. Detailed aspects and applications of FRAP technology are described in Kupferschmied et al. [11], Pfau et al. [12], Porecca et al. [13], Mansour et al. [14], however specific information for the current wind energy application are detailed below.

Requirements

The principal requirements for the probe were the capability to measure wind (speed, direction and turbulence parameters) in the atmospheric boundary layer and downstream of a wind turbine. Thus measurements in low dynamic head (0-10mbar), over large flow angles (≤ 70°), and with large bandwidth (≤1kHz) are required. A major challenge was to accomplish these with a measurement system that did not exceed the payload and autonomous flight limitations of the UAV, which was the chosen platform for high resolution flowfield measurements of full scale wind turbines. Moreover, the probe and sensor packaging needed to be robust, such that they can be reliably operated on a UAV.

Sensor Packaging

The sensing elements of the 7S-FRAP employ miniature pressure sensor dies (Intersema MS-7505-D), Fig. 1. This sensor is designed for low pressure applications (≤ 50mbar) that have stringent requirements on resolution and accuracy. Its sensor element consists of a silicon-micro-machined membrane bonded onto a Pyrex glass substrate. The pressure signal is proportional to the pressure difference between the back and the front side of the membrane, and is sensed by four implanted piezo-resistors.
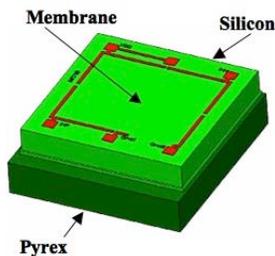

Fig. 1: Miniature pressure sensor die (Intersema MS-7505-D).

The sensor packaging and bonding techniques are derived from MEMS technology. These packaging and the bonding techniques ensure optimal spatial resolution, measurement bandwidth and protection of the sensors in harsh weather conditions. Moreover the gluing and bonding techniques employed in the present design provided a high degree of

reliability and low disturbance to the sensors as the probe can experience large temperature and pressure fluctuations.

As shown in Fig. 2, the miniature silicon piezo-resistive chip is glued onto a socket using a silicon glue with very low E-modulus. The silicon glue is based on an inorganic ground structure, which offers large temperature range of operation (-90 – 200°C) and is highly resistant to corrosive media. Thus the thermomechanical stresses are minimized. The photopolymer socket is encapsulated into a threaded casing of 5.5mm in diameter. The treated casing enables a repeatable fixation of the sensor in the probe tip, as well as the quick replacement of a sensor in case of a failure.
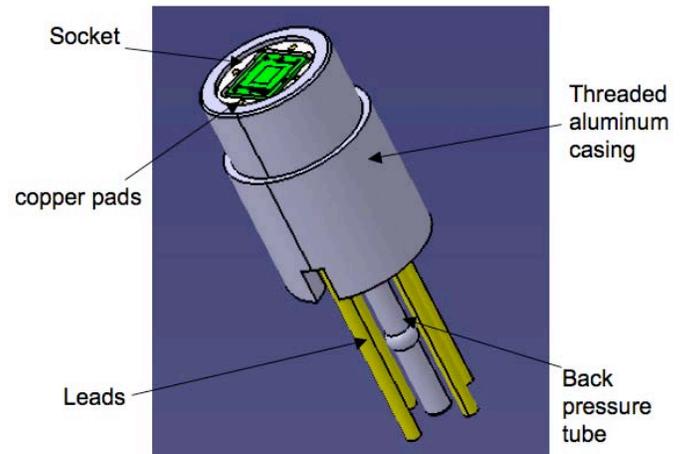

Fig. 2: Encapsulated pressure sensor die.

Probe Design

A close up view of 7S-FRAP probe's tip and its embedded differential pressure sensors are shown in Fig. 3. The 7S-FRAP consists of a 20mm hemispherical probe head that is comprised of 7 fast-response pressure sensors installed beneath the pressure taps. The sensing holes have a diameter of 1.3mm, which is less than one-twelfth of the probe diameter, ensuring negligible influence on the aero-calibration [15]. As the total and static pressures occur on the surface of an hemispherical probe at flow angles equal to 0° and about 45° respectively, the probe incorporates the surface pressure tapings at these positions with respect to the probe shaft axis. The volume and the length of pressure taps of the probe tip body are minimized, as these dimensions have a significant impact on the probe aerodynamics and measurement bandwidth. The reduction of the pressure tap volume is a key parameter to yield a high frequency measurement bandwidth as the eigenfrequency of the pneumatic cavity will affect the pressure sensor dynamic response. This issue will be discussed and quantified in the dynamic response section of this paper.
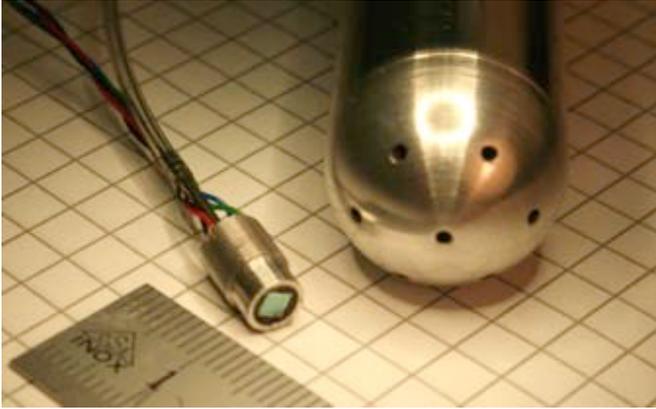
Fig. 3: 7S-FRAP probe tip and encapsulated pressure sensor.

The probe tip is installed on a cylindrical shaft to give an overall probe length of 70mm, which minimizes the potential field effect of the UAV on the probe's flowfield. The shaft has a squared-end, which enables the repeatable installation of the probe on the UAV.

Uninhabited Aerial Vehicle

In order to perform full-scale wind turbine measurements the 7S-FRAP probe is installed on a uninhabited aerial vehicle (UAV), Fig. 4.
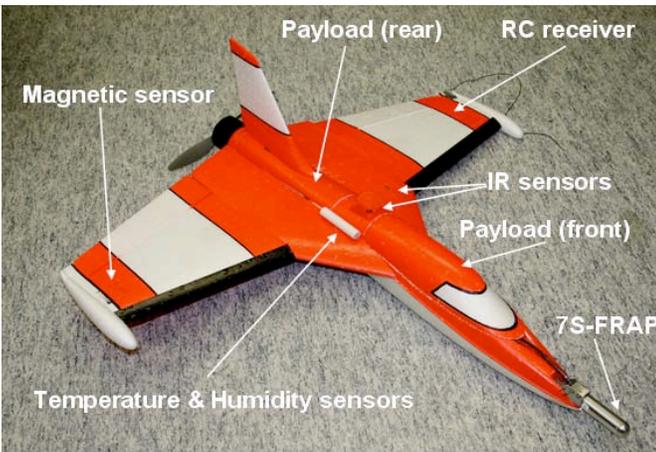

Fig. 4: Autonomous time-resolved wind measurement aircraft based on the model airframe "Funjet".

The "Funjet" airframe, manufactured by Multiplex, is of a pusher-prop configuration. The airframe is made of a very durable and easily repairable expanded polypropylene construction. It has a wingspan of 800mm and weighs 900g when fully instrumented. The propeller is driven by a brushless electric motor in order to reduce the vibrations that may affect the on-board sensors. As the airframe has limited payload bay area, therefore significant efforts have been put into the development of compact and light electronics and

avionics. The system is powered with a lithium battery that provides flight autonomy of approximately 25 minutes at a cruise speed of 15m/s.

Since remote pilot control is only possible within the range of sight and does not offer accurate and repeatable flight paths, the fully autonomous flight control system Paparazzi was used. Paparazzi is an open-source autopilot system oriented towards inexpensive autonomous aircraft [16, 17]. The Paparazzi system includes an on-board processor with its required sensors, autopilot software, a ground control station and a simulation environment to prepare and test the flight plans. The attitude is measured using a set of infrared thermopiles that sense the differential temperature between sky and ground. The altitude, the position as well as the ground speed are derived using a GPS receiver. The GPS provides a horizontal and vertical position accuracy of ±2.5m and ±5m, respectively. The ground speed accuracy is ±0.1m/s at 30m/s, with an error on the course heading of 0.5°.

In addition to the autopilot sensors, the UAV is equipped with sensors required to process the measurements from the 7-sensor fast-response aerodynamic probe. A magnetic sensor is installed to the UAV's sideslip angle. The magnetic sensor is placed at the tip of the wing fuselage to reduce distortion effects of the on-board electronics. The atmospheric pressure, used as the reference pressure for the fast-response differential pressure sensors of the 7S-FRAP, is measured via an absolute pressure sensor located in the rear compartment of the payload bay. In order to characterize accurately the atmospheric boundary layer profile and the work rate obtainable from measured wind profile, a sensor mounted externally on the side of the airframe measures temperature and humidity of the air.

The 7S-FRAP probe pressure signals are acquired simultaneously with a 24-bit resolution over a differential analog input range of ±2.2V and at a data sampling rate of 250Hz. However the on-board ADCs enable a data sampling frequency up to 3.4 kHz. The remaining on-board sensors are acquired with resolutions ranging from 12 to 16 bits. The data are stored in a binary format on an onboard multimedia flash card.

RESULTS

Static calibration

Fig. 5. shows the typical calibration raw data of the piezo-resistive sensor over a range of pressures 1-30mbar and temperatures 1-65°C. For the measurements, a fifth-order polynomial interpolation, Eq. 1 and Eq. 2 are used to determine the pressure and temperature from the measured sensor signals.

The measured sensitivities of the pressure sensor after amplification are 98 mV/mbar and 135 mV/K for the pressure signal and the temperature signal respectively. The noise on the pressure signal reduces the resolution of the analog-to-

digital converter to 19-bit effective, which provides a differential pressure measurement resolution of ±8.6 10⁻³ Pa. The calibration model exhibits an average standard deviation compared to the measured data of ±2.27 Pa and ±0.14K, which corresponds to an error of less than 0.075% and 0.018% over the full calibration range of the probe.
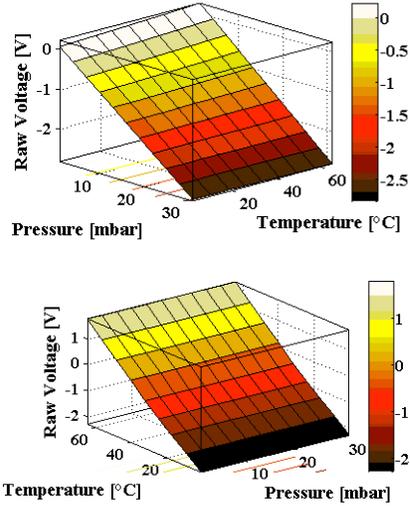

Fig. 5: Sensor static calibration data.

$$p(U, U_e) = \sum_{i=0}^{m} \sum_{j=0}^{n} K_{p_{i,j}} U^i U_e^j \qquad \textbf{Eq. 1}$$

$$T(U, U_e) = \sum_{i=0}^{m} \sum_{j=0}^{n} K_{T_{i,j}} U^i U_e^j \qquad \textbf{Eq. 2}$$
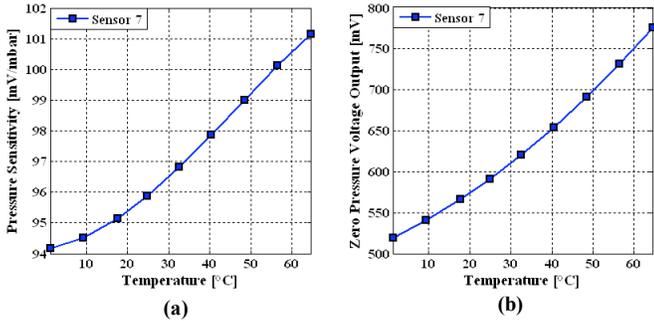

Fig. 6: (a) pressure sensitivity versus applied temperature, (b) zero pressure offset versus temperature.

As seen in Fig. 5 the output signal U is weakly temperature dependent, while the excitation signal U_e is decoupled from the pressure. However the effect of temperature on the pressure sensitivity, see Fig. 6.a and the zero pressure offset, which is the pressure signal output at zero applied pressure, see Fig. 6.b, is not negligible. The pressure signal output experiences 7.4% and 47% increase in pressure sensitivity and zero pressure output, respectively, when temperature varies from 1°C to 65°C. It can also be observed that the response to temperature variations is non-linear. Therefore the sensors require a calibration over the full range of intended temperature use.
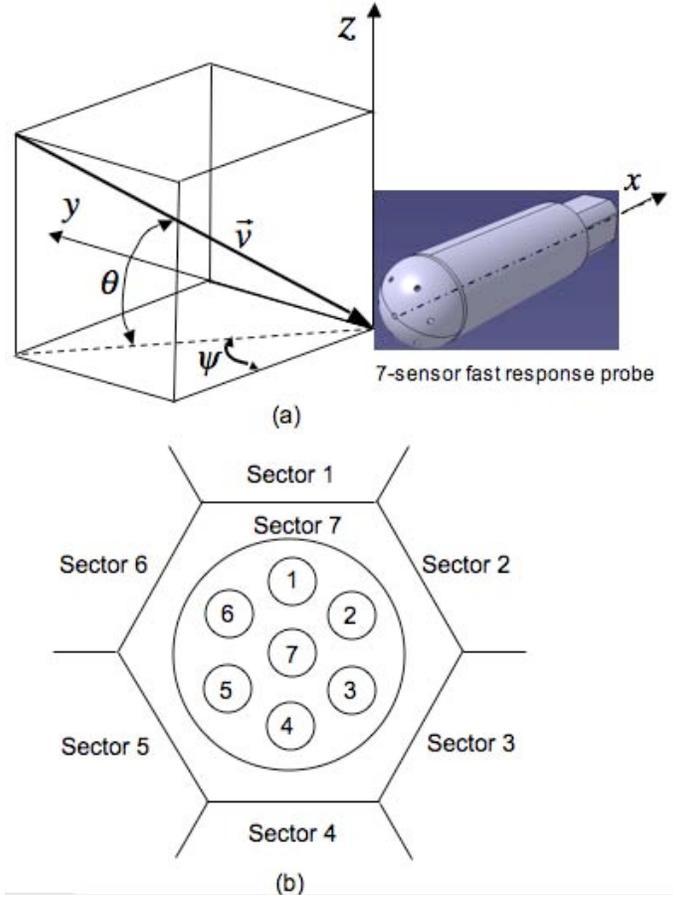
Aerodynamic calibration

Fig. 7: (a) Flow angles convention, (b) Pressure taps numbering and sectoring scheme.

The seven-sensor probe design is used to measure the wind over the high flow angle variations present in the turbulent boundary layer and in the wake of wind turbines. Fig. 7 shows (a) the definition of the flow angles and (b) the arrangement of the pressure taps. The probe is used in a non-nulling fashion and the pressure information from the seven sensors is combined to compute four pressure coefficients, representing the local yaw angle, ψ, pitch angle, θ, total pressure, P_o, and dynamic pressure q. This information is then used to derive the local velocity vector $\vec{v}$.

At low flow angles, the flow remains attached over the entire surface of the probe and the central port (n=7) has the highest pressure. Therefore the pressure measured by all seven sensors are used to determine the flow conditions. However at high flow angles, the flow separates on the leeward side of the probe and an off-center pressure sensor (n=1-6) has the highest pressure. In this case only a subset of the seven pressure sensors is used to determine the flow conditions, based on the sensor reading the highest pressure and the sensors that are adjacent to it. The difference between high and low flow angles leads to a sectoring scheme, which is employed in the current work as shown in Fig. 7.b.

The aero-calibration of the probe was made in the fully automated freejet facility at ETHZ. A detailed description of the facility can be found in [11]. The probe is installed on a three axis traversing system (lateral motion, yaw angle and pitch angle motion) in order to rotate the probe relative to the fixed jet. The automatic calibration procedure follows a pre-defined measurement grid for different probe yaw and pitch angles. For the low angle range the set of calibration data is taken on a homogenous grid that covers ±30° in yaw and pitch angles, for a Mach number of 0.07, that corresponds to a velocity of 25m/s.

Following an approach similar to that of Zilliac [18], a pitch angle coefficient, C_θ, is used to represent the local pitch angle, θ, and a tangential pressure-difference coefficient, C_ψ, is used to represent local yaw angle, ψ. Similar coefficients, C_o and C_q, are used to derive the total pressure and dynamic pressure, respectively. These coefficients are defined for low angles corresponding to sector 7 as follows:

$$C_{\theta,7} = \frac{2(P_4 - P_1) + (P_3 - P_6) - (P_2 - P_5)}{2(P_7 - \bar{P}_7)} \qquad \text{Eq. 3}$$

$$C_{\psi,7} = \frac{(P_3 - P_6) + (P_2 - P_5)}{\sqrt{3}(P_7 - \bar{P}_7)} \qquad \text{Eq. 4}$$

$$C_{o,7} = \frac{P_7 - P_o}{P_7 - \bar{P}_7} \qquad \text{Eq. 5}$$

$$C_{q,7} = \frac{P_7 - \bar{P}_7}{q} \qquad \text{Eq. 6}$$

$$\bar{P}_7 = \frac{1}{6}\sum_{n=1}^{6} P_n \qquad \text{Eq.7}$$

The polynomial curve-fit method of Gallington [19] is applied to the calibration data. Four sets of calibration coefficients are derived for the four flow properties (ψ, θ, C_o, C_q). The polynomial calibration coefficients $k_{ij\psi}$ and $k_{ij\theta}$, used to derive yaw and pitch flow angles, result from the solution of this set of linear equations using a least squares 10th order polynomial approximation, as shown in Eq. 8 and Eq. 7:

$$\psi = \sum_{i=0}^{n}\sum_{j=0}^{m} k_{ij\psi} C_\psi^i C_\theta^j \qquad \text{Eq. 8}$$

$$\theta = \sum_{i=0}^{n}\sum_{j=0}^{m} k_{ij\theta} C_\psi^i C_\theta^j \qquad \text{Eq. 7}$$

A similar procedure as for the flow angles is applied to the pressure measurements in order to derive the polynomial calibration coefficients for the total pressure and dynamic pressure. The relations Eq. 10 and Eq. 11 are a function of the computed flow yaw angle. The flow angles are converted into radians instead of degrees. The change of units into radians is more beneficial for calibration model accuracy. The polynomial interpolation order is 6 and 5 for total pressure and dynamic pressure, respectively.

$$C_o = \sum_{i=0}^{n}\sum_{j=0}^{m} k_{ijt} \psi^i \theta^j \qquad \text{Eq. 10}$$

$$C_q = \sum_{i=0}^{n}\sum_{j=0}^{m} k_{ijq} \psi^i \theta^j \qquad \text{Eq. 11}$$

The calibration curves of the 7S-FRAP probe are shown in Fig. 8 for ±30° in yaw and pitch, at a Mach number of Ma = 0.074 which corresponds to wind dynamic head and velocity of 4mbar and 27m/s, respectively.
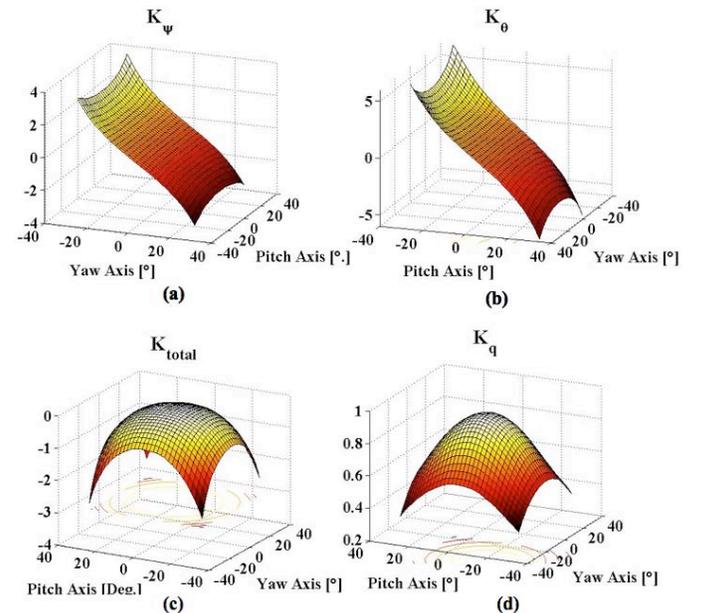

Fig. 8: Aero-calibration coefficients, (a) yaw flow angle, (b) pitch flow angle, (c) total pressure, (d) dynamic pressure.

Yaw Angle	Pitch Angle	Total Pressure	Dynamic Pressure
abs. [°] / rel. [%]	abs. [°] / rel. [%]	abs. [Pa] / rel. [%]	abs. [Pa] / rel. [%]
$5.75 \ 10^{-2}$ / $9.58 \ 10^{-2}$	$5.77 \ 10^{-2}$ / $9.62 \ 10^{-2}$	3.93 / $9.58 \ 10^{-1}$	2.35 / $5.72 \ 10^{-1}$

Table 1: Calibration model accuracy of the 7S-FRAP probe. Calibration range: Ma = 0.074, ±30° in yaw and pitch angles.
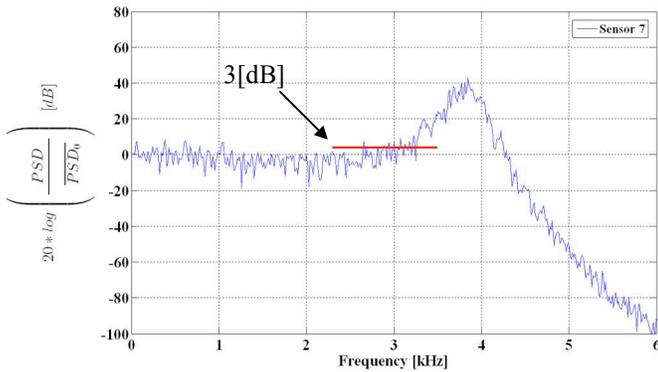
Dynamic Calibration

Fig. 9: Amplitude response of stagnation pressure sensor 7. The measured response is from grid generated turbulence.

The pneumatic cavity between the pressure tap and piezo-resistive sensor membrane can influence the unsteady pressure measurements. The acoustic resonance is associated with the characteristic length of the pneumatic cavity, implies that the measured signals around the eigenfrequency of the pneumatic cavity are strongly amplified and have a phase shift [20]. It is thus important to quantify the eigenfrequency of the newly design shielded pressure tap. This eigenfrequency determines the frequency measurement bandwidth of 7S-FRAP probe.

The dynamic response of the pneumatic cavity was measured in the freejet facility, equipped with a fine mesh grid. The resulting flow turbulence has a constant amplitude over relatively low frequencies and then decays with a characteristic slope of -5/3 at higher frequencies. The amplitude response in terms of PSD/PSD_0 versus frequency is shown in Fig. 9. The peak at 3.8kHz corresponds with the eigenfrequency of the pneumatic cavity of the stagnation pressure sensor 7, which exhibits the largest pneumatic cavity of all seven sensors. The amplitude is flat up to a frequency of 3kHz, above which the amplitudes are in excess of 3dB. Thus the cutoff frequency of 3kHz determines the bandwidth of the 7S-FRAP probe.

Atmospheric Boundary Layer Measurements
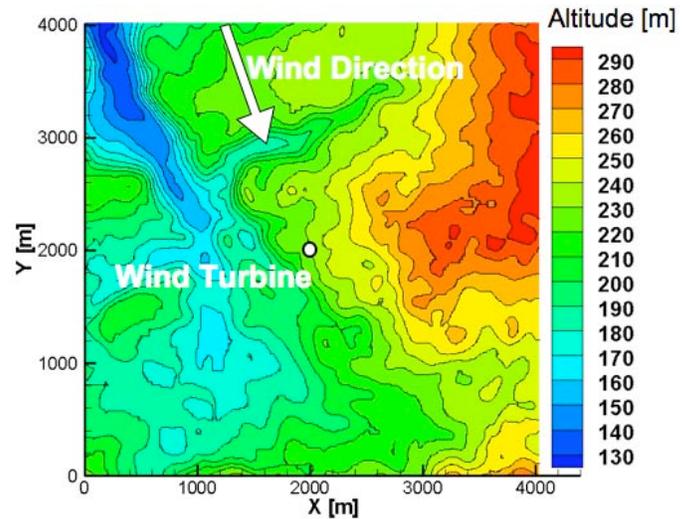
Flight Plan and Measurement Approach

Fig. 10: Elevation map of wind turbine location, showing the predominant wind direction over the measurement campaign.
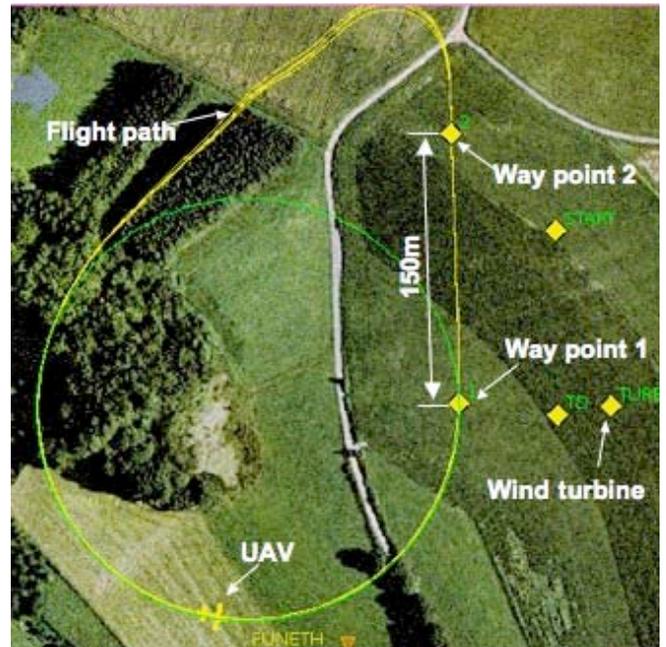

Fig. 11: Flight pattern during time-resolved wind measurements performed upstream of a Vestas V80 wind turbine.

The atmospheric boundary layer upstream of a Vestas V80 wind turbine was measured using the 7-sensor FRAP. The wind turbine is located in Extertal, Germany. This 2.0MW turbine has a rotor blade diameter of 80m, with a hub

height of 100m. The cut-in and cut-out wind speeds are 4m/s and 25m/s respectively. The nominal rotational speed of the rotor is 16.7rpm and is geared up through a planetary/helical stage gearbox for electricity generation.

The vegetation and the climate of this location are representative of the "Weserbergland" region (Weser highland). As shown in Fig. 10, the wind turbine stands at an altitude of 240m in close proximity to a hill reaching a maximum elevation of 370m. The orographic characteristics are quiet complex, the landscape is characterized by a tangle of hills and valleys that drain streams into the Weser River. The atmospheric conditions are often influenced by depressions that stretch from the north-northwest in the direction of Extertal. During the present measurement campaign the predominant wind direction was from 340° north, as shown in Fig. 10.

As shown in Fig. 11 the wind turbine is located an area dotted with small forests and open agricultural terrain. Shown also in Fig. 11 is plan view of the flight path of the UAV. The flight path is comprised of a 150m long, straight, horizontally level measurement section between waypoints 1 and 2, followed by a sharp left bank turn immediately after waypoint 2, then a more gradual left turn along an arc of a circle ahead of waypoint 1. Along this closed loop-shaped pattern measurements were made over a height (relative to ground) of 80m to 200m, with a height resolution of 15m. The gradual turn ahead of waypoint 2 allowed controlled ascents to be made to successive measurement heights.
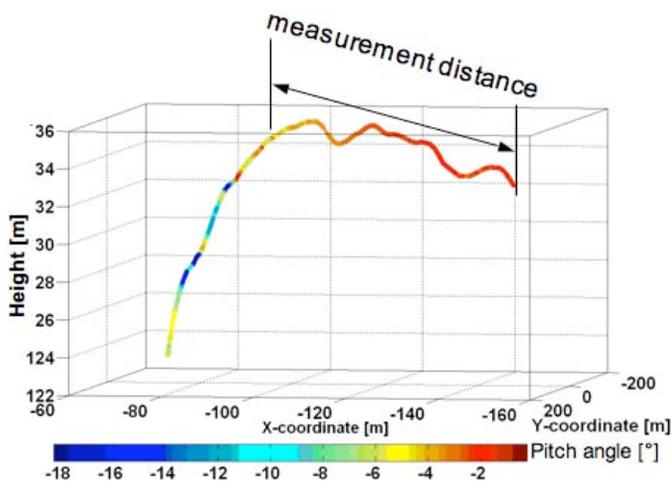

Fig. 12: Flight pattern between waypoints 1 and 2 during measurement at 125m above the ground. The color indicates the measured pitch angle.

Between waypoints 1 and 2, the UAV is flown at a constant altitude and with constant throttle. The 7S-FRAP probe thus measured the time-resolved true air speed. Therefore the time resolved wind velocity is derived from the difference between the true air speed and the ground speed, which is derived from the on-board GPS. Fig. 12 shows a representative flight pattern between waypoints 1 and 2. The

colors along the flight path indicate the measured pitch angle, that is derived from the 7-sensor FRAP. Over the measurement section the actual altitude varies from 132m to 135m, which is within the vertical resolution (±5m) of GPS. The measured pitch is in the range of -5° to 0°. Therefore as shown in Fig. 12 the measurement distance considered for wind speed measurement is covering only the portion where the UAV has reached a stable level flight condition both in terms of height and pitch angle.

Measurement Results

The time averaged wind profile measurement using the newly developed 7S-FRAP probe is compared and assessed with an independent set of measurements performed with the UAV using the more established circle-flight technique. The circle-flight measurement technique has been previously used for several atmospheric boundary layer measurement campaigns as described by Reuder et al. [10]. The basic operating principle of the circle-flight measurement is to fly the UAV in a circular pattern such that the ground speed is decelerated by headwind on the first half of the circle and accelerated by tailwind on the other half of the circle. As the UAV is operated with constant throttle, the wind speed can be determined from the difference between minimum and maximum ground speeds over the full circle.

Fig. 13 shows the 10 minute-averaged wind speed that is measured on the nacelle of the wind turbine during the 7S-FRAP (20 minutes duration from 14:10 to 14:30Hrs) and circle-flight (20 minutes duration from 15:10 to 15:30) different measurement periods. The nacelle is equipped with an ultrasonic anemometer to measure wind speed and the uncorrected wind speed data are shown. The two sets of measurements performed upstream of the wind turbine are within 40min time interval. The dashed blue area shows the 7S-FRAP measurement time, whereas the red-dashed indicates the UAV-circle flight measurement time. However although the measurement periods are relatively close to each other as shown in Fig. 13, the wind averaged velocity decreased from 3.6m/s to 2.45m/s between the two respective measurements. This is a challenge in making field measurements on full-scale wind turbines. Thus at LEC, a sub-scale wind turbine facility in which model wind turbines can be tested at full-scale non-dimensional in controlled conditions is used as a complement to the present work [21].

Two measurement legs were performed during the 7S-FRAP measurement period, with 10 minutes interval between the two measured wind profiles. As shown in Fig.13 the wind conditions were not similar for the three sets of wind profile measurements. Therefore Fig.14 shows the atmospheric boundary layer wind velocity profiles, measured by the 7S-FRAP and the UAV-circle flight techniques, non-dimensionalized with the measured wind speed at 200m. Quantitatively the first and second 7S-FRAP profiles are in a good agreement with each other, which proves a good measurement repeatability of the F7S-FRAP. The three

profiles show a strong accelerated flow over the height range of 100 - 175m with a peak velocity located around 150m, which is about 20% higher than the measured wind velocity at 200m. The wind turbine's nacelle anemometer wind velocities are also shown in Fig. 14. The uncorrected wind velocities measured at 100m by the nacelle anemometer are of 23% and 22% lower than the 7S-FRAP first measurements and the UAV-circle flight measurements performed at 95 and 102m, respectively. This is in good agreement with the general assumption that a modern rotor with a maximum power coefficient of 0.45 retards the wind speed behind the rotor plane by approximately 25%, [22].
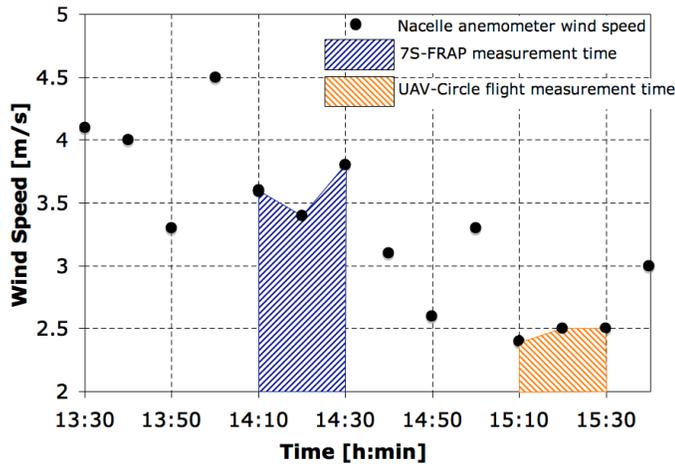

Fig. 13: 10 minute-averaged uncorrected wind speed measured by the wind turbine nacelle's anemometer. Blue and red dashed areas represent the 7S-FRAP and UAV circle-flight wind profile measurement time.
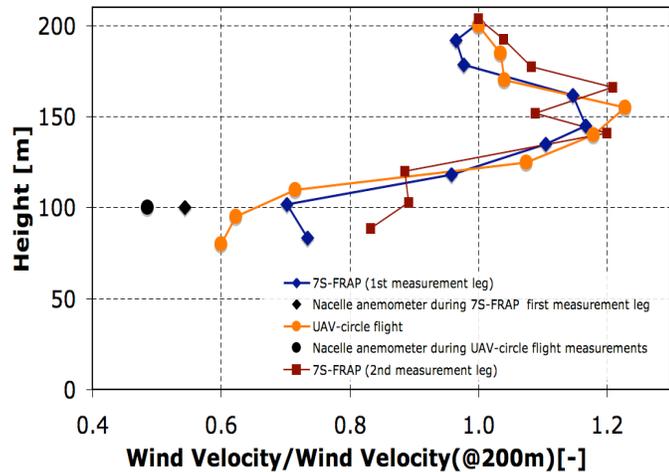

Fig. 14: Profiles of wind speed from 7S-FRAP and UAV circle-flight measurements. The nacelle anemometer averaged data are indicated with black markers. All wind velocity are non-dimensionalized with the wind velocity measured at 200m

Fig. 15 shows the profile of the mean wind speed measured during the first measurement leg of the 7S-FRAP together with its respective maximum and minimum wind profile based on the standard deviation of the time-resolved wind speed measurements. Also shown in Fig. 15 is the logarithmic wind profile that is derived using Eq. 12. This profile is representative of a site assessment analysis in the commonly used approach of met masts equipped with cup-anemometers.

$$\overline{v}_H = \overline{v}_{ref} \frac{\ln \dfrac{H}{z_o}}{\ln \dfrac{H_{ref}}{z_o}} \qquad \textbf{Eq. 12}$$

The averaged wind speed $\overline{v}_{ref}$ measured by the 7S-FRAP at the height H_{ref} = 83m is used as a reference value. A roughness length z_o = 0.15 which corresponds to roughness class of 2 has been used for the open agricultural terrain [22]. It can be observed that the logarithmic height profile gives an unsatisfactory assessment of the wind profile at this location. As the wind turbine is installed on an elevated plateau the wind profile experiences a local acceleration, due to a venturi effect, over the heights 100-175m approximately. The logarithmic wind profile underestimates the wind speed up to 32% at 145m. As the wind power varies as the cube of wind speed, the estimated power is in error by up to 96%.
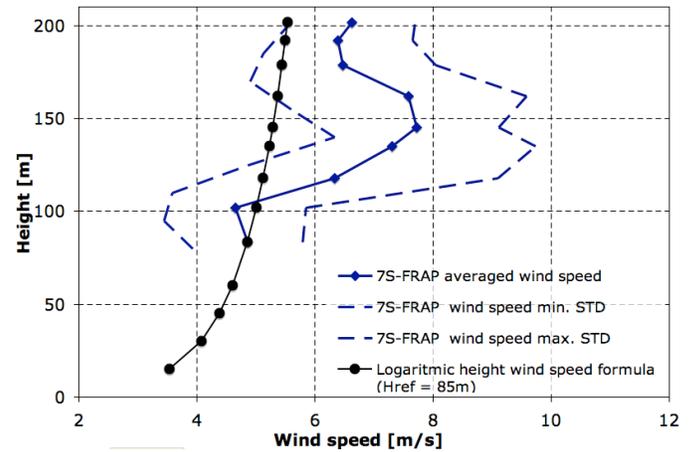

Fig. 15: Profile of wind speed measured with 7S-FRAP with its maximum and minimum wind speed based on the standard deviation of time-resolved wind speed. The black line shows the logarithmic wind profile based on the reference wind velocity measured at 85m.

As shown in Fig. 15 the measured wind profile shows that there is a strong shear around the wind turbine hub height (100m). The maximum wind speed is at 145m and is 48% higher than the average speed at 83m. The profile exhibits as well the highest levels of fluctuations in the range of 100 to

175m, with a maximum fluctuation of 2.76m/s at 118m. At this height the measured velocity fluctuations represent a 44% variation around the average speed. It can be therefore anticipated that a wind turbine at this location experiences cyclic and stochastic loads variations on the turbine blades. Therefore the design of the turbine must capable of sustaining these load variations with time, in order that the fatigue life of the turbine components covers the expected service life.

Another consequence of the shear in the wind profile is a variation in incidence, and its associated loading, on the rotor blades. As the blade pitch is constant during a rotor revolution, the variation in velocity across the boundary layer means that the loading varies cyclically. During the 7S-FRAP measurement time the average wind turbine rpm and the blade pitch angle were in the range of 10.5 ± 0.5 rpm and $1° \pm 0.5°$. Fig. 16 shows the velocity triangles at mid-span ($r/R = 0.5$) for heights of 83 and 118m. Due to the strong wind shear the incidence changes from 8.2° at 83m to 15° at 118m, which are the respective bottom and top positions the blade mid-span section. The Vestas-V80 wind turbine blades has a NACA 63-xxx blade profile at mid-span [23]. The exact blade profile is unknown, but several related reports describe studies on a NACA 63-415 or similar profiles [24]. The maximum lift coefficient for this profile is 1.5 at incidences around 13°. For the 118m height the 15° incidence leads to a lift coefficient of 1.28, whereas the lift coefficient at 83m decreases to 1.13. Therefore, there is a 12% variation in the section lift between these two heights.
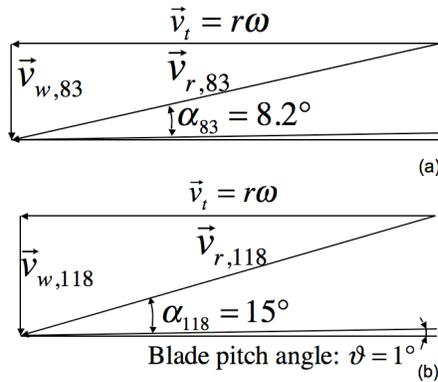

Fig. 16: Velocity triangles for a span position r/R = 0.5 (a) at H = 83m, (b) H = 118m.

CONCLUDING REMARKS

A novel measurement approach for wind energy applications that is comprised of an autonomous UAV, which is equipped with a seven-hole fast-response aerodynamic probe is developed and demonstrated. The electric-powered UAV is equipped with an autopilot system that consists of an on-board flight & data processor, infrared sensors for attitude control, and GPS receiver for position information, in order to provide 25 minutes autonomous flight with high spatial

resolution (~6.3% of rotor diameter) of measurements around full-scale wind turbines. The fast-response aerodynamic probe has 7 miniature pressure sensors, which are packaged, integrated and calibrated as a light, compact measurement system using techniques that have been developed and pioneered at ETH Zurich in its development of fast-response measurement techniques over the last 20 years. A lightweight, on-board ADC with 24-bit resolution and maximum sampling rate of 3.4 kHz, together with a high precision absolute pressure sensor for the measurement of the reference ambient pressure and a magnetic sensor for measurement of sideslip angle complete the measurement chain. Static calibration of the F7S-UAV probe's sensors yield an average standard deviation of ±2.27 Pa, which corresponds to less than 0.075% error over the full calibration range of the probe. The aerodynamic calibration yields less than 0.1% relative error in angles and total pressure, and a dynamic calibration shows the measurement bandwidth of the present design is 3kHz.

The time-averaged wind profile from the F7S-UAV probe is found to be in very good agreement to a wind profile that is measured using circle flights of the UAV. This time-averaged profile, which is measured at a wind turbine that is located in moderately complex terrain, differs by as much as 30% from the wind profile that is extrapolated from a logarithmic height formula; therefore the limited utility of extrapolated profiles, which are commonly used in site assessments, is made evident. A comparison of the nacelle height time-averaged wind speeds shows that there is a 23% reduction in the wind speed, which is in very good agreements with the expected reduction for a modern wind turbine.

The time-varying wind profiles show that, at a given height, the velocity fluctuations can be as much as 44% of the time-averaged velocity, therefore indicating that the wind turbine and its components, notably the gearbox, will experience substantial non-cyclic loads that may impact the fatigue life of the components. Furthermore, the shear in the velocity profile also subjects the fixed pitch blade to varying incidences and cyclic load variations. Analysis of the associated velocity triangles indicates that the sectional lift coefficient at mid-span of this modern turbine would vary by 12% in the measured time-averaged wind profile. These variations must be accounted in the structural design of the blades. Thus the measurements of the unsteady wind profile accomplished with this novel measurement system, demonstrate that it is a cost effective complement to the suite of available site assessment measurement tools.

REFERENCES

[1] L. Kristensen, "The Perennial Cup Anemometer," *Wind Energy,* vol. 2, pp. 59-75, 1999.

[2] D. A. Smith, M. Harris, A. S. Coffey, T. Mikkelsen, H. E. Joergensen, J. Mann, and R. Danielan, "Wind LIDAR Evaluation at the Danish Wind Test Site in Hovsore," in *EWEC 2004*, London.

[3] M. Courtney, R. Wagner, and P. Lindelöw, "Testing and Comparison of LIDARs for Profile and Turbulence Measurements in Wind Energy," in *14th International Symposium for the Advancement of Boundary Layer Remote Sensing*: IOP Conf. Series: Earth and Environment Science 1, 012021, 2008.

[4] R. Frehlich and N. Kelley, "Measurements of Wind and Turbulence Profiles with Scanning Doppler Lidar for Wind Energy Applications," *IEEE Trans. Geosci. Remote Sens. ,* vol. 1, pp. 42-47, 2008.

[5] R. M. Huffaker, A. V. Jelalian, and J. A. Thomson, "Laser-Doppler System for Detection of Aircraft Trailing Vortices," in *IEEE*, 1970, pp. 322-326.

[6] C. M. Shun, "Ongoing Research Has Lead to Improved Wind Shear and Turbulence Alerts," *ICAO J.,* vol. 58, pp. 4-6, 2003.

[7] S. Hannon, K. Barr, J. Novotny, J. Bass, A. Oliver, and M. Anderson, "Large Scale Wind Resource Mapping Using a State-of-the-Art 3D Scanning Lidar," in *European Wind Energy Conference & Exhibition*, Brussels, Belgium, 31 Mars - 3 April, 2008, pp. 1-7.

[8] T. Mikkelsen, J. Mann, M. Courtney, and M. Sjöholm, "Windscanner: 3-D wind and Turbulence Measurements from Three Steerable Doppler Lidars," in *14th International Symposium for Advancement of Boundary Layer Remote Sensing*, IOP, Ed.: IOP Conf. series: Earth and Envirnmental Science 1, 012018, 2008.

[9] T. Spiess, J. Bange, M. Buschmann, and P. Vörsmann, "First Application of The Mini-UAV 'M^{2}AV'," *Meteorologische Zeitschrift,* vol. 16, pp. 159-169, 2007.

[10] J. Reuder, P. Brisset, M. Jonassen, M. Mueller, and S. Mayer, "SUMO: A Small Unmanned Meteorological Observer for Atmospheric Boundary Layer Research," in *14th International Symposium for the Advancement of Boundary Layer Remote Sensing, IOP Conf. Series: Earth Environ. Sci., 1 012014*, Riso, 23-25 June, 2008.

[11] K. Kupferschmied, P. Köppel, C. Roduner, and G. Gyarmathy, "On The Development and Application of the FRAP (Fast-response Aerodynamic Probe) System for Turbomachines- Part 1: The Measurement System," *J. Turbomachinery,* vol. 122, pp. 505-516, 2000.

[12] A. Pfau, J. Schlienger, A. I. Kalfas, and R. S. Abhari, "Virtual Four Sensor Fast Response Aerodynamic Probe (FRAP) ," in *16th Bi-Annual Symposium on Measuring Techniques in Transonic and Supersonic Flows in Cascades and Turbomachines*, Cambridge, UK, Sept. 23-24, 2002.

[13] L. Porecca, M. Hollenstein, A. I. Kalfas, and R. S. Abhari, "Turbulence Measurements and Analysis in a Multistage Axial Turbine," *J. Propulsion and Power,* vol. 23, pp. 227-234, 2007.

[14] M. Mansour, N. Chokani, A. I. Kalfas, and R. S. Abhari, "Time-Resolved Entropy Measurements Using a Fast Response Entropy Probe " *Meas. Sci. Technol.,* vol. 10 p. 115401 (14pp), 2008.

[15] D. W. Bryer and R. C. Pankhurst, *Pressure-Probe Methods for Determining Wind Speed and Flow Direction*: Her Majesty's Stationary Office, London, 1971.

[16] P. Brisset, A. Drouin, M. Gorraz, P.-S. Huard, and J. Tyler, "The Paparazzi Solution," in *MAV2006*, Sandestin, Florida, November 2006.

[17] M. Mueller and A. Drouin, "Paparazzi - the Free Autopilot. Build your Own Uav," in *24th Chaos Communication Congress*, Berliner Congress Center, December 27-30, 2007.

[18] G. G. Zilliac, "Modelling, Calibration, and Error Analysis of Seven-Hole Pressure Probes," *Exp. Fluids,* vol. 14, pp. 104-120, 1993.

[19] R. W. Gallington, "Measurement of Very Large Flow Angles with Non-Nulling Seven-Hole Probe," *Aeronautics Digest,* vol. USAFA-TR-80-17, pp. 60-88, 1980.

[20] C. Gossweiler, H. J. Humm, and P. Kupefrschmied, "The Use of Piezo-Resistive Semi-Conductor Pressure Transducers for Fast-Response Probe Measurements in Turbomachinery," in *Proc. 10th Symposium on Measuring Techniques for Transonic and Supersonic Flows in Cascades and Turbomachines*, Brussels, 1989.

[21] S. Barber, Y. Wang, N. Chokani, and R. S. Abhari, "The Effect of Ice Shapes on Wind Turbine Performance," in *13th International Workshop on Atmospheric Icing of Structures* Andermatt, Switzerland, 2009.

[22] E. Hau, *Wind Turbines: Fundamentals, Technologies, Applications, Economics*: Springer-Verlag Berlin, 2006.

[23] C. Hochart, "Simulation Numérique et Expérimentale de l'Ecoulement d'Air et de l'Accrétion de Glace

autour d'une Pale d'Eolienne ": MS thesis, Univérsité de Québec, 2007.

[24] C. Bak, P. Fuglsang, J. Johansen, and I. Antoniou, "Wind Tunnel Tests of the NACA 63-415 and a Modified NACA 64-415," Risø National Laboratory, Roskilde, Denmark 2000.